Comparative analysis of the effects of tantalum doping and annealing on atomic layer deposited $(Ta_2O_5)_x(Al_2O_3)_{1-x}$ as potential gate dielectrics for GaN/Al$_x$Ga$_{1-x}$N/GaN high electron mobility transistors

T. Partida-Manzanera,[1,2,a)] J. W. Roberts,[1] T. N. Bhat,[2] Z. Zhang,[2] H. R. Tan,[2]
S. B. Dolmanan,[2] N. Sedghi,[1] S. Tripathy,[2] and R. J. Potter[1]

[1]*Centre for Materials and Structures, School of Engineering, University of Liverpool, Liverpool, L69 3GH, United Kingdom*
[2]*Institute of Materials Research and Engineering, A*STAR (Agency for Science, Technology and Research), Innovis, 2 Fusionopolis way, Singapore 138634*

This paper describes a method to optimally combine wide band gap Al_2O_3 with high dielectric constant (high-κ) Ta_2O_5 for gate dielectric applications. $(Ta_2O_5)_x(Al_2O_3)_{1-x}$ thin films deposited by thermal atomic layer deposition (ALD) on GaN-capped $Al_xGa_{1-x}N$/GaN high electron mobility transistor (HEMT) structures have been studied as a function of the Ta_2O_5 molar fraction. X-ray photoelectron spectroscopy shows that the bandgap of the oxide films linearly decreases from 6.5 eV for pure Al_2O_3 to 4.6 eV for pure Ta_2O_5. The dielectric constant calculated from capacitance-voltage measurements also increases linearly from 7.8 for Al_2O_3 up to 25.6 for Ta_2O_5. The effect of post-deposition annealing in N_2 at 600 °C on the interfacial properties of undoped Al_2O_3 and Ta-doped $(Ta_2O_5)_{0.12}(Al_2O_3)_{0.88}$ films grown on GaN-HEMTs has been investigated. These conditions are analogous to the conditions used for source/drain contact formation in gate-first HEMT technology. A reduction of the Ga-O to Ga-N bond ratios at the oxide/HEMT interfaces is observed after annealing, which is attributed to a reduction of interstitial oxygen-related defects. As a result, the conduction band offsets (CBOs) of the Al_2O_3/GaN-HEMT and $(Ta_2O_5)_{0.16}(Al_2O_3)_{0.84}$/GaN-HEMT samples increased by $\sim$1.1 eV to 2.8 eV and 2.6 eV, respectively, which is advantageous for n-type HEMTs. The results demonstrate that ALD of Ta-doped Al_2O_3 can be used to control the properties of the gate dielectric, allowing the κ-value to be increased, while still maintaining a sufficient CBO to the GaN-HEMT structure for low leakage currents. © *2016 AIP Publishing LLC*. [http://dx.doi.org/10.1063/1.4939298]

I. INTRODUCTION

Due to their superior material properties, group III-nitride semiconductors have attracted much attention in the past few years as candidates for next generation high-frequency, high-power, and high-temperature power switching devices. Power transistors are used in a wide range of consumer electronics, converting mains voltages down to end-user low voltages. The efficiency of current Si-based devices shows limitations related to Si voltage blocking capability, operation temperature, and switching frequency. GaN-based devices have the potential to overcome these limitations due to GaN wide band gap, high breakdown voltage, high charge density, high electron mobility, and high thermal conductivity.[1,2] Furthermore, GaN-on-Si technology offers a cost effective route towards the commercially viable high-performance GaN-based power electronics. Recent advances are now allowing the successful growth of high quality GaN-based epitaxial layers on top of large area Si substrates despite the large lattice mismatch and thermal expansion coefficient mismatch between GaN and Si.[3–7] Among GaN devices, $Al_xGa_{1-x}N$/GaN high electron mobility transistors (HEMTs) are the most prevalent structure for power device applications due to the superior transport

properties provided by the highly conductive two-dimensional electron gas (2DEG) formed below the $Al_xGa_{1-x}N$/GaN interface. This is a result of the difference in band gap of the two materials and spontaneous and piezoelectric polarization effects.[8,9] One of the main limitations of these structures is the high gate leakage currents through the Schottky barrier[10] caused by a low Schottky barrier height and/or poor interface quality between the gate metal and the nitride.[11] To address this problem, wide bandgap/high dielectric constant (high-κ) materials have been investigated as gate dielectrics for metal-oxide-semiconductor HEMT (MOS-HEMT) structures. Due to its self-limiting behavior, atomic layer deposition (ALD) meets the needs for the deposition of very thin, conformal and highly insulating high-quality gate oxides in the sub-nanometer range for ultra-scaled microelectronic devices. In addition to this, the ALD process is not limited by the substrate area size and it can be integrated with GaN-based device processing of 200 nm GaN-on-Si wafers in a complimentary metal-oxide-semiconductor (CMOS) foundry.

In literature, wide bandgap high-κ oxides such as Al_2O_3,[12,13] HfO_2,[14,15] and ZrO_2[16] deposited by ALD as gate dielectrics for $Al_xGa_{1-x}N$/GaN MOS-HEMTs have shown low gate leakage currents. Among these, ALD Al_2O_3 is one of the most widely investigated candidates as a high-κ gate dielectric for GaN-based devices due to its large band gap

a)Electronic mail: sgtparti@liv.ac.uk

(6.5 eV),[17] large breakdown electric field (5–10 MV/cm),[18] and ease of deposition. However, its relatively small dielectric constant ($\kappa \sim 9$)[19] limits further scaling of the equivalent oxide thickness (EOT). For this reason, the introduction of a higher dielectric constant material such as tantalum oxide (Ta_2O_5), with a dielectric constant typically around 25 for amorphous Ta_2O_5,[20] may allow a further reduction of the gate leakage while maintaining or enhancing the device gate capacitance. Ta_2O_5 is a key high-κ material for next generation MOS due to its high breakdown electric field (4.5 MV), low leakage current ($<10^{-8}$ A/cm^2 at 1 MV/cm) and good step coverage.[21–23] Moreover, Ta_2O_5 used as gate dielectric in capacitors fabricated on GaN has shown low fixed oxide charge density and low midgap interface trap density.[24] However, the higher κ value of Ta_2O_5 compared with Al_2O_3 comes at the expense of a smaller band gap (~4.4 eV)[25,26] and hence lower conduction and valence band offsets. To achieve a high driving current capability, the gate dielectric must have a sufficient conduction band offset (for n-MOS devices) or valence band offset (for p-MOS devices) to the underlying semiconductor in order to prevent carrier leakage. Small band offsets can result in high leakage due to Schottky emission over the barrier and due to enhanced Fowler-Nordheim tunneling at high voltages. Furthermore, from a device application point of view, one of the most challenging requirements for the integration of high-κ oxides as gate dielectrics is the chemical and thermal stability of the oxide film at the interface with the underlying semiconductor and the control of interface trap defects. In the case of gate-first HEMT technology where high temperature annealing steps are required for source/drain contact formation during device processing, it is important to understand the effects of post-deposition annealing in the gate oxide and its interfacial properties at the nitride surface. Changes in the band offsets between high-κ oxides and GaN due to band bending after annealing have been reported.[27] These changes can affect device performance especially if the resultant band offsets are smaller than 1 eV.[28] In addition, the lower crystallization temperature of Ta_2O_5 can result in the recrystallization of the gate oxide during annealing at temperatures above 600 °C,[28,29] inducing high leakage currents due to grain boundary conduction. Previous research has been carried out on the band offsets between Al_2O_3 and GaN.[30,31] However, there are no reports on the characteristics of Ta-doped $(Ta_2O_5)_x$ $(Al_2O_3)_{1-x}$ films on GaN or GaN/Al_xGa_{1-x}N/GaN HEMT structures. To optimally combine the complementary characteristics of Al_2O_3 and Ta_2O_5, we studied the bandgap (E_g), band offsets, and κ value of ALD $(Ta_2O_5)_x(Al_2O_3)_{1-x}$ layers as a function of x as well as the impact of post-deposition annealing on these properties. This paper presents for the first time a comparative analysis of the effects of Ta-doping and annealing on the interfacial properties and thermal stability of undoped Al_2O_3 and Ta-doped $(Ta_2O_5)_{0.12}(Al_2O_3)_{0.88}$ grown on GaN-capped Al_xGa_{1-x}N/GaN HEMT structures.

II. EXPERIMENTAL DETAILS

Al_xGa_{1-x}N/GaN HEMT structures were grown on a 1.0 mm thick 200 mm diameter Si(111) substrate (supplied by MRS, prime grade) using an AIXTRON CCS metal organic chemical vapor deposition (MOCVD) system. The total thickness of the nitride stack is about 4.3 μm. It includes a $\sim$400 nm thick AlN nucleation layer, three step-graded Al_xGa_{1-x}N intermediate layers with a total thickness of approximately 1.8 μm, a $\sim$1.8 μm carbon-doped GaN buffer layer, and a $\sim$300 nm undoped GaN channel. The top HEMT structure consists of a thin AlN spacer, a $\sim$18–19 nm $Al_{0.24}Ga_{0.76}$N barrier layer, and a $\sim$4.0 nm top undoped thin GaN cap. Prior to ALD, the HEMT samples were treated with an *exsitu* wet-chemical cleaning process. The samples were sonicated in separate acetone and isopropanol (supplied by Sigma-Aldrich®, 99.5% purity) for 10 min each to remove organic contaminants and then rinsed in DI water for 2 min and dried with compressed nitrogen.

Ta-doped Al_2O_3 films were deposited at 250 °C using an Oxford Instruments OpAL thermal ALD reactor. Electronic grade trimethylaluminium (TMA) and pentakis(dimethylamino)tantalum (PDMAT) (supplied by SAFC Hitech®) were used as the aluminum and tantalum sources, respectively, whereas DI water was used as the oxygen containing co-reactant. The TMA and H_2O were both held at room temperature and delivered using vapor draw, whereas the PDMAT was heated to 75 °C and was transported with the assistance of 100 sccm of argon (BOC 99.998%) using a dip-leg bubbler. The self-limiting growth rates for the Al_2O_3 and Ta_2O_5 ALD processes were obtained by measuring the film thicknesses using high-resolution scanning transmission electron microscopy (HR-STEM) and dividing the thickness by the total number of ALD cycles (n = 120). The deposition rates of Al_2O_3 and Ta_2O_5 were calculated to be 0.9 Å/cycle and 0.8 Å/cycle, respectively, in agreement with other published work.[32,33] Tantalum doping of Al_2O_3 was realized using delta doping where TMA based ALD cycles (n_{TMA}) (20 ms TMA dose/5 s purge/20 ms H_2O dose/5 s purge) were periodically interspersed with PDMAT ALD cycles (n_{PDMAT}) (4 s PDMAT dose/5 s purge/20 ms H_2O dose/5 s purge). Throughout the process, the overall argon flow into the reactor was maintained at 200 sccm giving a chamber pressure of approximately 200 mTorr. The overall number of ALD cycles (n) was set to 60 to deposit $\sim$5 nm thick films for band alignment and interface studies. $\sim$10 nm thick samples were grown using n = 120 cycles to investigate the composition and bandgap of the bulk oxide films.

Post deposition rapid thermal annealing (RTA) was performed using Jipelec JetFirst 150 rapid thermal processing system. The samples were annealed at 600 °C for 60 s under nitrogen ambient, which is analogous to the conditions used for the formation of ohmic contacts in the GaN-based HEMT structures using an Au-free Ta/Al/Ta metallization scheme.[34,35] X-ray photoelectron spectroscopy (XPS) measurements were performed using a VG ESCALAB 200i-XL system equipped with a monochromatic Al Kα x-rays (1486.7 eV). All peak binding energies were referenced to the C 1s peak at 285.0 eV to compensate for surface charging. The data analysis of the XPS spectra was carried out using AVANTAGE software, including curve fitting and determination of the oxides composition using Scofield sensitive factors and transmission functions provided by the instrument manufacturer for the O 1s, Al 2p, and Ta 4f
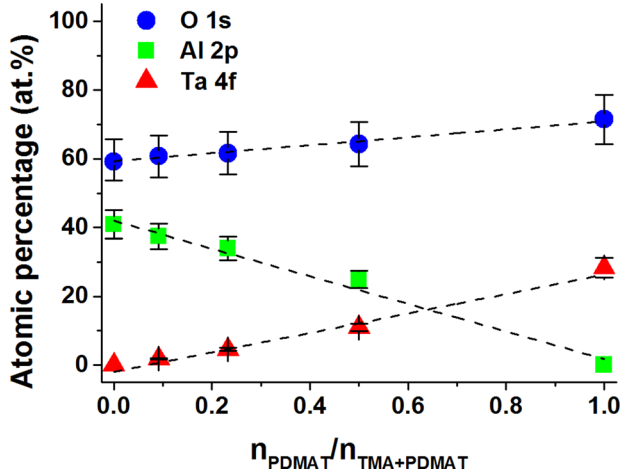
FIG. 1. Atomic percentage of the O 1s, Al 2p, and Ta 4f core level spectra obtained by XPS for the $\sim$10 nm thick $(Ta_2O_5)_x(Al_2O_3)_{1-x}$ samples as-deposited and after annealing in N_2 at 600 °C for 60 s, as a function of the PDMAT precursor ALD cycle fraction.

peaks. Cross-sectional TEM images were acquired using a FEI Titan 80–300 kV scanning transmission electron microscope operating at 200 kV in high-angle annular dark field STEM (HAADF-STEM) and high-resolution bright-field TEM (HR-BFTEM) modes.

n-type Si(100) substrates (supplied by PI-KEM Ltd., test grade) were also used for the fabrication of Au/oxide/Si(100) MOS capacitors to measure the oxide films dielectric properties. Capacitance-voltage (CV) measurements were carried out using an E4980A precision LCR meter. Gold top electrodes of $\sim$1 mm diameter were deposited by sputtering through a shadow mask. After annealing at 600 °C for 60 s in nitrogen (BOC Zero grade), the back metal contact was formed by evaporation of Al on the backside of the Si substrate. The capacitors received a forming gas anneal at 430 °C for 30 min to reduce the density of interface states (D_{it}).[36] The dielectric constant of the oxide films was calculated using the following relationship:

$$\kappa = \frac{C_{ox} \, t_{ox}}{\varepsilon_0 \, A}, \tag{1}$$

where t_{ox} is the gate oxide thickness in m, A is the device area in m^2, $\varepsilon_0 = 8.85 \times 10^{-12}$ F/m, and C_{ox} is the oxide capacitance in F. C_{ox} was obtained using a series capacitance

model assuming a 15 Å thick SiO_2 interlayer between the oxide films and the Si substrate as given by the following relationship:

$$\frac{1}{C} = \frac{1}{C_{SiO_2}} + \frac{1}{C_{ox}}, \tag{2}$$

where C is the measured n-MOS capacitance in the accumulation region and C_{SiO2} is the capacitance of the SiO_2 layer.

III. RESULTS AND DISCUSSION

A. Composition and bandgap of ALD $(Ta_2O_5)_x(Al_2O_3)_{1-x}$ layers

The composition of the $\sim$10 nm thick "bulk" oxide films before and after annealing was investigated by XPS analysis of the peaks area, binding energy, and full width at half maximum (FWHM) of the O 1s, Al 2p, and Ta 4f core level spectra. The composition of the samples as a function of the Ta ALD cycle fraction is shown in Fig. 1.

XPS results show that the percentage of the different elements in the samples varies linearly with the Ta ALD cycle fraction. Furthermore, the atomic ratios fit closely with the expected stoichiometry of $(Ta_2O_5)_x(Al_2O_3)_{1-x}$. A summary of the elemental compositions as well as the value of the Ta_2O_5 molar fraction, x, are given in Table I. It can be observed that the annealing process has no significant effect on composition.

The bandgap energies of the "bulk" oxide samples were calculated by measuring the difference between the core level peak energy and the onset of energy loss from the XPS O 1s core level energy-loss spectra.[37] The bandgap of as-deposited and annealed $(Ta_2O_5)_x(Al_2O_3)_{1-x}$ oxide films as a function of the Ta_2O_5 mole fraction is shown in Fig. 2.

The bandgap of the $(Ta_2O_5)_x(Al_2O_3)_{1-x}$ samples decreases linearly with the Ta_2O_5 fraction, and no significant changes are observed after annealing. The bandgap of pure Al_2O_3 is found to be 6.5 eV for the as-deposited and annealed samples, which is in good agreement with literature values of 6.5 eV reported for amorphous Al_2O_3 grown by ALD.[27,38] This value is significantly smaller than the band gap of 8.8 eV measured for bulk Al_2O_3 crystal,[39] which has been attributed to the presence of unoccupied states associated with oxygen vacancies that act as electron and hole traps within the bandgap.[40] The value obtained for

TABLE I. Atomic percentage of the O 1s, Al 2p, and Ta 4f core level spectra obtained by XPS for the $\sim$10 nm thick $(Ta_2O_5)_x(Al_2O_3)_{1-x}$ samples as-deposited and after annealing in N_2 at 600 °C for 60 s.

	As-deposited			Annealed			
$n_{PDMAT}/n_{TMA+PDMAT}$	O 1s (at. %)	Al 2p (at. %)	Ta 4f$_{7/2}$ (at. %)	O 1s (at. %)	Al 2p (at. %)	Ta 4f$_{7/2}$ (at. %)	Ta_2O_5 mole fraction value, x, as in $(Ta_2O_5)_x(Al_2O_3)_{1-x}$
0	59.1	40.9	…	59.7	40.3	…	0
0.09	60.8	37.4	1.8	60.7	37.5	1.8	0.05
0.23	61.6	33.9	4.5	61.7	33.7	4.6	0.12
0.50	64.3	24.9	10.9	64.3	24.8	10.9	0.30
1	71.6	…	28.4	71.5	…	28.5	1

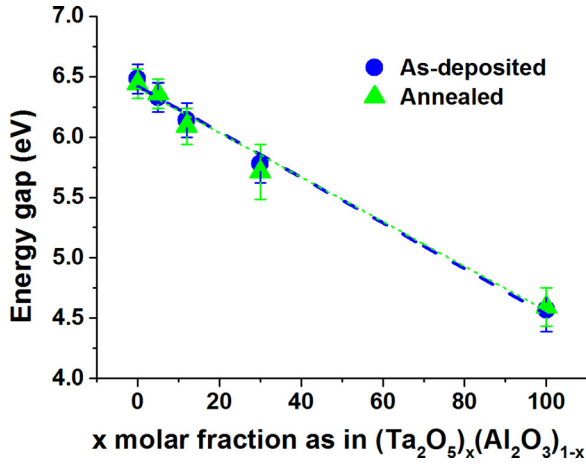FIG. 2. Bandgap of as-deposited and annealed $\sim$10 nm thick $(Ta_2O_5)_x$ $(Al_2O_3)_{1-x}$ layers as a function of the molar fraction, x.

the Ta_2O_5 films before and after annealing is 4.6 eV, which is close to previously reported values of $\sim$4.5 eV for amorphous Ta_2O_5 deposited by ALD.[20] This value is within the range of optical band gap values reported for crystalline Ta_2O_5 ($\sim$3.9–4.5 eV) and amorphous Ta_2O_5 ($\sim$4.2–5.3 eV), which depend on the growth method.[41] From linear fitting, the value of the bandgap (E_g) for $(Ta_2O_5)_x(Al_2O_3)_{1-x}$ can be derived by the following equation:

$$E_g = 6.45 - 1.80\,x. \qquad (3)$$

B. Dielectric constant of ALD $(Ta_2O_5)_x(Al_2O_3)_{1-x}$ layers

To examine the impact of the introduction of tantalum on the electrical properties of the Ta-doped samples, the dielectric constant of the $\sim$10 nm thick $(Ta_2O_5)_x(Al_2O_3)_{1-x}$ layers grown on Si(100) was calculated as a function of the Ta_2O_5 molar fraction from CV measurements at 100 kHz as shown in Fig. 3.

The dielectric constant increases linearly with the Ta_2O_5 molar fraction, x. The calculated dielectric constant values determined for the $x = 0$ and $x = 1$ samples are 7.8 and 25.6, respectively, which are comparable to the literature values of
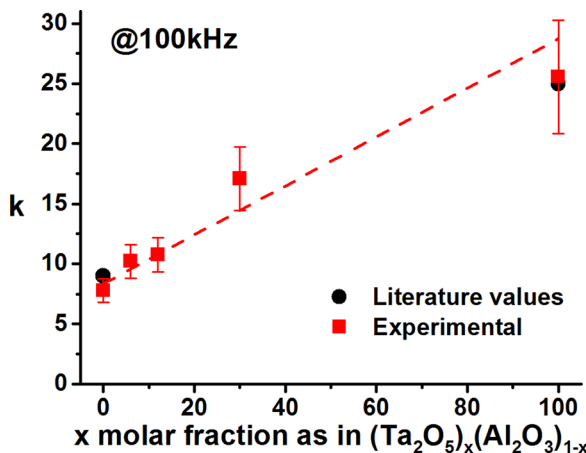
$\sim$9 and $\sim$25 known for Al_2O_3 and Ta_2O_5, respectively.[19,20] The results suggest a significant increase in the dielectric constant of the $(Ta_2O_5)_x(Al_2O_3)_{1-x}$ layers with the introduction of Ta.

C. Band offsets of Al_2O_3 and $(Ta_2O_5)_{0.12}(Al_2O_3)_{0.88}$ gate dielectrics on GaN/AlGaN/GaN-HEMT structure

A comparative analysis of the impact of tantalum doping on the gate oxides and their interface with the GaN-HEMT was carried out for two samples: undoped Al_2O_3 and $(Ta_2O_5)_{0.16}$ $(Al_2O_3)_{0.84}$. These samples were selected based on preliminary band alignment studies of $(Ta_2O_5)_x(Al_2O_3)_{1-x}$ films grown on GaN-on-Si substrate to ensure sufficient valence band offset (VBO) and conduction band offset (CBO) between the oxide films and GaN ($>$1 eV).

The VBO of the ALD oxide layers on the GaN-based HEMT structure were determined by XPS using the method proposed by Grant[42] and Kraut *et al.*[43]

$$\Delta E_V = (E_{CL,GaN} - E_{V,GaN}) - (E_{CL,oxide} - E_{V,oxide}) + E_{CL}, \qquad (4)$$

where E_{CL} represents the binding energy of the core levels (CL) and E_V is the binding energy of the valence band maximum (VBM). $E_{CL,GaN}$ and $E_{V,GaN}$ are the CL and the VBM binding energies of the GaN-HEMT substrate, $E_{CL,oxide}$ and $E_{V,oxide}$ are the CL and the VBM binding energies of the bulk oxide film, and ΔE_{CL} is the difference between the CL binding energies of the GaN-HEMT substrate and the oxide in the oxide/GaN-HEMT interface. In this analysis, the XPS binding energies of the Ga-N bond and Al 2p are used as the core levels of bulk GaN-HEMT substrate and oxides, respectively. According to Poisson's equation, band bending is caused by the spatially varying electrostatic potential which bends all of the bands or energy levels by an amount that depends only on the distance from the interface. Therefore, the $(E_{CL} - E_V)$ values should be independent of band bending because the VBM and CL bands are affected equally. The only parameter that is influenced by band bending and polarization effect is ΔE_{CL}.

The difference between the binding energy of the Ga-N bond and the VBM in the GaN-HEMT, $E_{CL,GaN} - E_{V,GaN}$, is investigated from the Ga 3d and VBM spectra obtained for the uncoated HEMT substrate as shown in Fig. 4.

The Ga 3d core level XPS spectrum (Fig. 4(a)) has been deconvoluted into two components corresponding to Ga-N
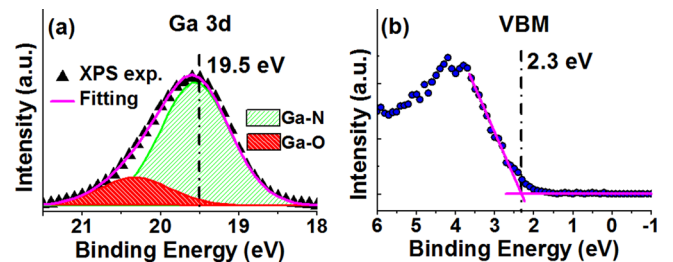

FIG. 3. Dielectric constant values calculated as a function of the Ta_2O_5 molar fraction, x, for the $\sim$10 nm thick $(Ta_2O_5)_x(Al_2O_3)_{1-x}$ films grown on Si(100) at the frequency of 100 kHz.

FIG. 4. XPS spectra of (a) Ga 3d core level and (b) VBM obtained for the uncoated GaN/$Al_{0.24}Ga_{0.76}$N/GaN-HEMT structure. The core level of the Ga 3d peak and the VBM are indicated with dashed lines.

and Ga-O bonds. The Ga-O spectrum can be attributed to oxidation of the GaN surface when the epilayers are exposed to air due to the vacuum break following MOCVD.[44] The VBM is determined by extrapolating the leading edge of the valence band spectrum (Fig. 4(b)) to the base line.[45] The binding energy difference between the Ga-N bond and VBM in the GaN-HEMT substrate is 17.2 eV, which is slightly less than values obtained from electronic-state studies of bulk GaN samples where the Ga 3d core level is 17.7–17.8 eV below the VBM.[46,47] This slight reduction is attributed to the presence of growth induced in-plane stress in the nitride epilayer HEMT stack due to the difference in lattice parameters and thermal expansion coefficients between the GaN cap and the underlying AlGaN. This stress can have a significant influence on the electronic band structure thus leading to a variation in the VBM.[48]

The difference between the binding energy of the Al 2p core level and the VBM in the "bulk" oxide layers, $E_{CL,oxide} - E_{V,oxide}$, is investigated from the Al 2p and VBM spectra of the ~10 nm thick oxide films (shown in the supplemental material).[49] The term $(E_{CL} - E_V)_{oxide}$ is determined from the Al 2p and VBM obtained for the ~10 nm thick "bulk" oxide layers. For the Al_2O_3 sample the binding energy of the Al 2p core level is found to be 71.0 eV below the VBM. This value is within the range of values of 70.4 eV and 71.8 eV reported in other studies for bulk Al_2O_3.[27,30,31] The value obtained for the $(Ta_2O_5)_{0.12}(Al_2O_3)_{0.88}$ sample is 71.1 eV, showing that the addition of Ta doping has little effect on the difference between the core levels of Al 2p and VBM. After annealing the $(E_{CL} - E_V)_{oxide}$ value does not vary for any of the samples, which is in agreement with Poisson's prediction.

The difference between the binding energies of the Ga-N bond and the Al 2p core levels at the interface, ΔE_{CL}, is obtained for the ~5 nm thick Al_2O_3 and $(Ta_2O_5)_{0.12}(Al_2O_3)_{0.88}$ layers grown on the GaN-HEMT. The Ga 3d and Al 2p core level spectra of the as-deposited and annealed samples are shown in Fig. 5.

The results indicate that the band bending is altered during post deposition annealing. The Al 2p and Ga 3d core levels shift to higher energies after annealing by ~0.8 eV and ~1.9 eV, respectively. The value of ΔE_{CL} for the as-deposited Al_2O_3/GaN-HEMT sample is measured to be 55.2 eV, which according to Eq. (4) gives a VBO of 1.5 eV. This value is significantly smaller than the experimental value of 1.8 eV reported by other authors,[27] similar to the theoretical values of 1.7 eV calculated from the electron affinity model[50] and the charge neutrality level (CNL) model when the GaN and Al_2O_3 CNLs are calculated by local density approximation (LDA).[51] However, the Al_2O_3/GaN VBO calculated using CNLs values for GaN and Al_2O_3 determined empirically is 1.4 eV, which is closer to the value obtained experimentally in this study.[52] The value of ΔE_{CL} measured for the as-deposited $(Ta_2O_5)_{0.16}(Al_2O_3)_{0.84}$/GaN-HEMT sample is 55.1 eV, corresponding to a VBO of 1.2 eV, which implies that the addition of Ta to Al_2O_3 results in a reduction of 0.3 eV with respect the VBO of undoped Al_2O_3 on the GaN-HEMT. This reduction is within the expected limits considering the smaller theoretical VBO value of 1.1 eV calculated for Ta_2O_5 on GaN using the LDA
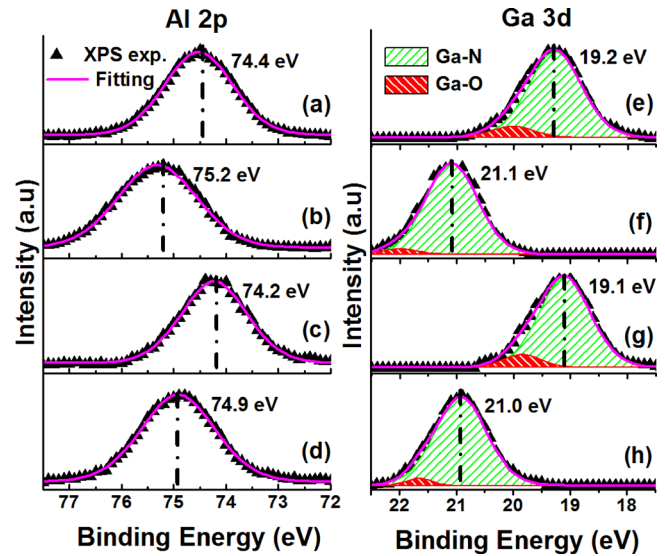

FIG. 5. XPS Al 2p spectra of: (a) ~5 nm Al_2O_3/GaN-HEMT as deposited, (b) ~5 nm Al_2O_3/GaN-HEMT annealed, (c) ~5 nm $(Ta_2O_5)_{0.12}(Al_2O_3)_{0.88}$/GaN-HEMT as deposited, and (d) ~5 nm $(Ta_2O_5)_{0.12}(Al_2O_3)_{0.88}$/GaN-HEMT annealed; and Ga 3d spectra of: (e) ~5 nm Al_2O_3/GaN-HEMT as deposited, (f) ~5 nm Al_2O_3/GaN-HEMT annealed, (g) ~5 nm $(Ta_2O_5)_{0.12}(Al_2O_3)_{0.88}$/GaN-HEMT as deposited, and (h) ~5 nm $(Ta_2O_5)_{0.12}(Al_2O_3)_{0.88}$/GaN-HEMT annealed. The values of the core level of the peaks are indicated with dashed-dotted lines.

and CNL model.[53] After annealing, the binding energy difference between Al 2p and Ga 3d core levels decreases by ~1.1 eV, resulting in VBOs of 0.3 eV and 0.1 eV for the annealed Al_2O_3/GaN-HEMT and $(Ta_2O_5)_{0.16}(Al_2O_3)_{0.84}$/GaN-HEMT, respectively. This reduction in the VBOs indicates that this annealing process significantly changes the band alignment between the dielectrics and the GaN-HEMT.

The CBOs between the oxide films and the GaN-based heterostructure can be derived by the following equation:

$$\Delta E_C = E_g - \Delta E_V - 3.4 \,(\text{eV}), \qquad (5)$$

where 3.4 eV is the bandgap of GaN,[54] confirmed experimentally by photoluminescence spectroscopy. The bandgap values determined for the Al_2O_3 and $(Ta_2O_5)_{0.12}(Al_2O_3)_{0.88}$ layers, as well as their valence and conduction band offsets with the GaN-HEMT structure before and after annealing in N_2 at 600 °C for 60 s are listed in Table II. The results show a reduction of 0.1 eV in the CBO of the Ta-doped sample with respect to the undoped Al_2O_3, which indicates that the reduction of the CBO due to the introduction of Ta-dopant is smaller compared to the reduction of 0.3 eV observed for the VBO. Fig. 6 shows a schematic of the energy band diagrams determined by XPS for the as-deposited and annealed Al_2O_3/GaN-HEMT and $(Ta_2O_5)_{0.12}(Al_2O_3)_{0.88}$/GaN-HEMT interfaces. The annealing process step significantly alters the band offsets at the dielectric/nitride interfaces, reducing the VBOs and increasing the CBOs, giving higher barrier heights in the n-type HEMTs.

D. Ga-O to Ga-N ratio at the GaN surface

A reduction in the Ga-O to Ga-N peak area ratio is observed for the interface samples with respect to the

TABLE II. Summary of the $(E_{CL} - E_V)_{oxide}$, ΔE_{CL}, ΔE_v, E_g, and ΔE_C values for the Al_2O_3 and $(Ta_2O_5)_{0.12}(Al_2O_3)_{0.88}$ layers and the GaN-HEMT structure, before and after annealing in N_2 at 600 °C for 60 s.

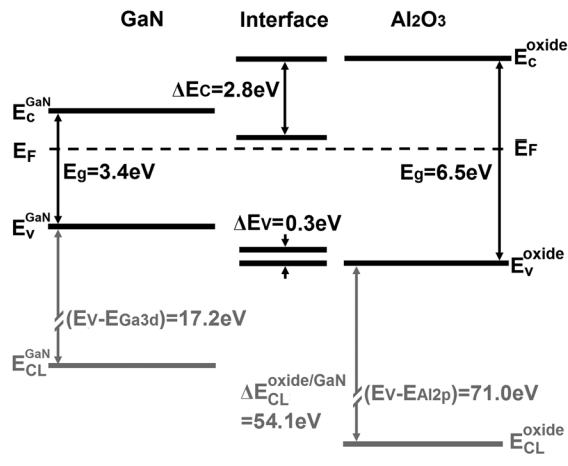| Samples	$(E_{CL}-E_V)_{oxide}$ (eV)	ΔE_{CL} (eV)	ΔE_V (eV)	E_g (eV)	ΔE_C (eV)
As-deposited Al_2O_3	71.0	55.2	1.5	6.5	1.6
Annealed Al_2O_3	71.0	54.1	0.3	6.5	2.8
As-deposited $(Ta_2O_5)_{0.12}(Al_2O_3)_{0.88}$	71.1	55.1	1.2	6.1	1.5
Annealed $(Ta_2O_5)_{0.12}(Al_2O_3)_{0.88}$	71.1	50.0	0.1	6.1	2.6

uncoated GaN-HEMT sample. The Ga-O/Ga-N peak area ratio calculated for the uncoated GaN-HEMT sample is 0.23, whereas the Ga-O/Ga-N area ratios of as-deposited Al_2O_3 and $(Ta_2O_5)_{0.12}(Al_2O_3)_{0.88}$ films grown on the GaN-HEMT structure are 0.11 and 0.10, respectively. This reduction in the Ga-O bond concentration is consistent with the "self-cleaning" effect previously observed when Al_2O_3 is grown by ALD on GaAs,[55] InGaAs,[56] and AlGaN,[57,58] which suggests the passivation of the oxide surface by the metal precursor during deposition. Al_2O_3 surface passivation in GaN-based MOS-HEMTs is expected to reduce the number of negative electronic surface states. In addition to reducing the gate leakage current, this decrease in surface states can mitigate current collapse caused by the formation of a virtual gate arising from negative charge injection from the gate edges.[59] Additionally, the Ga-O/Ga-N peak area ratios of the annealed Al_2O_3 and $(Ta_2O_5)_{0.12}(Al_2O_3)_{0.88}$ samples further reduce to 0.04 for both samples. This "clean up" effect after annealing has previously been reported on ALD ZrO_2 grown on GaN.[60] The decrease in the Ga-O to Ga-N peak area after annealing appears to lead to an increase of the Ga-N bond binding energy (Fig. 5(b)) which suggests that the
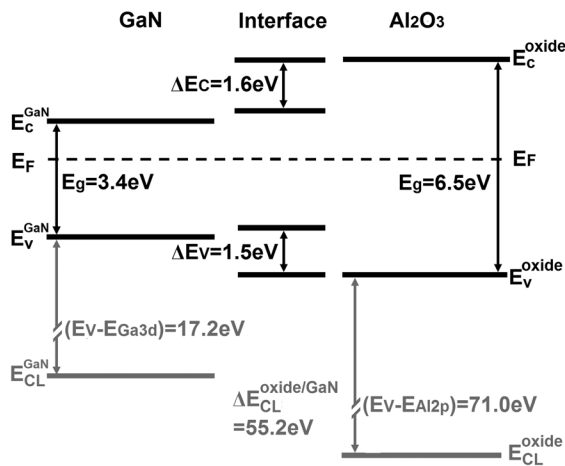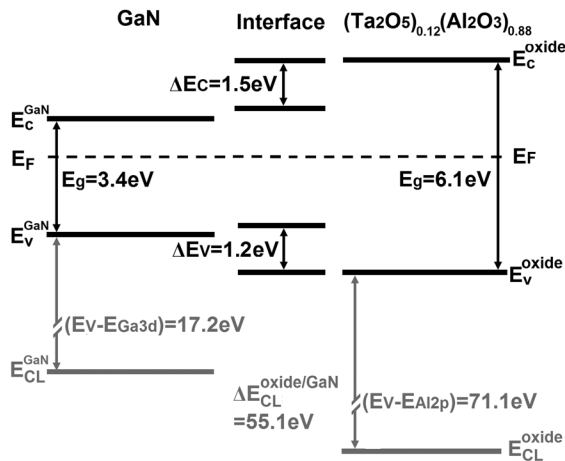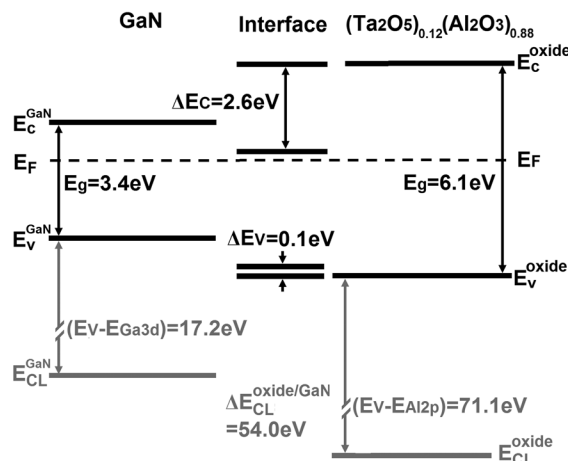

FIG. 6. Energy band diagrams determined by XPS for (a) Al_2O_3/GaN-HEMT interface as deposited, (b) Al_2O_3/GaN-HEMT interface annealed, (c) $(Ta_2O_5)_{0.12}(Al_2O_3)_{0.88}$/GaN-HEMT interface as deposited, and (d) $(Ta_2O_5)_{0.12}(Al_2O_3)_{0.88}$/GaN-HEMT interface annealed. The valence band offset (ΔE_V), conduction band offset (ΔE_C), GaN-HEMT core level (E_{CL}^{GaN}), oxide core level (E_{CL}^{oxide}), and the core level separation across the interface (ΔE_{CL}) are represented.

Fermi-Level position at the GaN surface is affected by surface-related defects states associated with GaO_x. Oxygen interstitial defects have been shown to act as deep acceptors in Al_2O_3/GaN structures.[61] Spontaneous polarization in GaN leads to a negative bound polarization charge at the GaN surface and ionized donors to compensate these defects,[62] which results in upward band bending at the GaN surface and lower Ga-N bond binding energy. The shifts of the Ga-N bond to higher binding energies after annealing can therefore be attributed to the reduction of oxygen defects at the GaN surface, which is in agreement with the results obtained.

E. Cross section and thermal stability of Al_2O_3 and $(Ta_2O_5)_{0.12}(Al_2O_3)_{0.88}$ gate dielectrics on GaN/AlGaN/GaN-HEMT structure

The cross-sectional HAADF-STEM images of the $\sim$5 nm thick Al_2O_3 and $(Ta_2O_5)_{0.12}(Al_2O_3)_{0.88}$ layers grown on the GaN-HEMT structure before and after annealing are shown in Figs. 7(a)–7(d). As the HEMT structure is grown on a 200 mm diameter Si(111) substrate, a small variation in AlGaN barrier and GaN cap thicknesses is expected across the wafer.
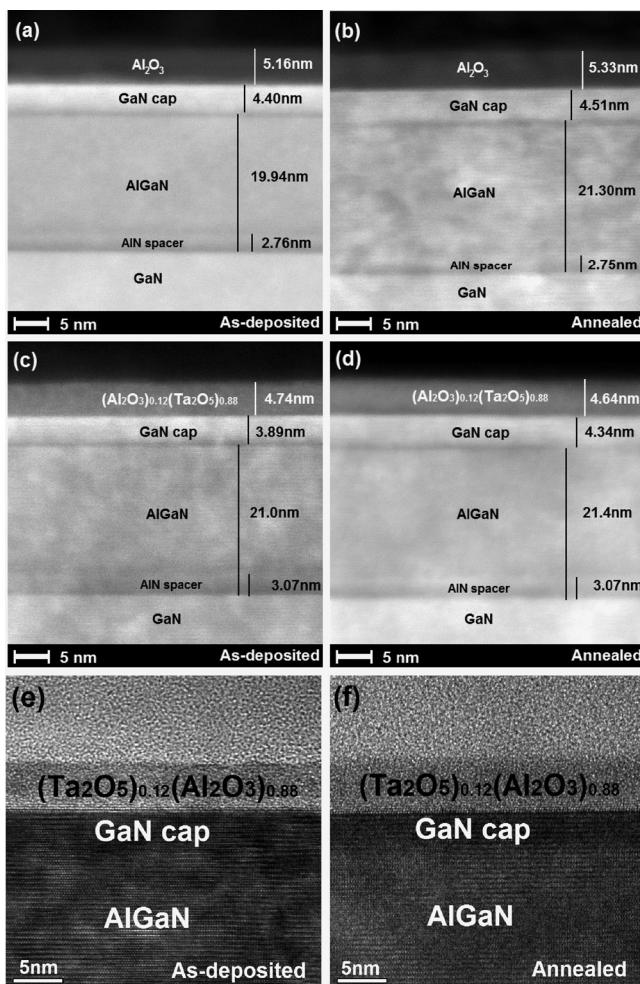

FIG. 7. (a)–(d) Cross-sectional HAADF-STEM of as-deposited and annealed Al_2O_3 and $(Ta_2O_5)_{0.12}(Al_2O_3)_{0.88}$ layers grown on the GaN/$Al_{0.24}Ga_{0.76}$N/GaN HEMT structure highlighting the top ALD oxide, GaN cap, AlGaN barrier, and AlN spacer on GaN buffer layers. (e) and (f) represent cross-sectional HR-BFTEM of the as-deposited and annealed $(Ta_2O_5)_{0.12}(Al_2O_3)_{0.88}$ layers grown on top of such HEMT structures.

HAADF-STEM imaging shows a continuous and sharp interface of the ALD oxide films and the GaN cap layer. The oxide film thickness is uniform for both the as-grown and annealed sets of samples. In order to further investigate any Ta-doping induced inhomogeneity at the interfaces, HR-BFTEM was performed for the HEMT samples coated with the $\sim$5 nm thick $(Ta_2O_5)_{0.12}(Al_2O_3)_{0.88}$ layers before and after annealing (Figs. 7(e) and 7(f)). The as-deposited and annealed samples show a similar morphology in terms of the amorphous nature of the oxide layers. The interfaces show a good thermal stability after RTA at 600 °C in N_2, with a sharp and very flat transition from crystalline GaN to amorphous oxide with no obvious interfacial layer. There appears to be a slight improvement in the interface abruptness of the $(Ta_2O_5)_{0.12}(Al_2O_3)_{0.88}$ oxide layers and the GaN-HEMT structure after RTA. The TEM results therefore prove that the introduction of Ta does not affect the thermal stability of the investigated $(Ta_2O_5)_{0.12}(Al_2O_3)_{0.88}$ oxide film during the annealing process used in the present study.

IV. CONCLUSIONS

Ta doping has been used to improve the dielectric constant of Al_2O_3 as a gate dielectric for GaN-HEMT structures. XPS measurements show that the composition of the ALD-$(Ta_2O_5)_x$ $(Al_2O_3)_{1-x}$ films has good stoichiometry and varies linearly with the Ta ALD cycle fraction. The bandgap of the oxide layers decreases linearly with the Ta_2O_5 molar fraction, x, from 6.5 eV for pure Al_2O_3 to 4.6 eV for pure Ta_2O_5. The calculated dielectric constant value from CV measurements also varies linearly with the x molar fraction, increasing from 7.8 for Al_2O_3 up to 25.6 for Ta_2O_5. The interfacial properties of Al_2O_3 and $(Ta_2O_5)_{0.12}(Al_2O_3)_{0.88}$ layers grown on GaN-capped $Al_{0.24}Ga_{0.84}$N/GaN-HEMT structures have been analyzed before and after annealing in N_2 at 600 °C. HR-TEM results show that the introduction of Ta does not affect the thermal stability of the doped $(Ta_2O_5)_{0.12}(Al_2O_3)_{0.88}$ film. From XPS the VBOs of as-deposited Al_2O_3/GaN-HEMT and $(Ta_2O_5)_{0.12}$ $(Al_2O_3)_{0.88}$/GaN-HEMT are 1.5 eV and 1.2 eV, respectively, with corresponding CBOs of 1.6 eV and 1.5 eV. After annealing, both samples are characterized by a reduction of defects or excess interstitial oxygen at the oxide/nitride interface. This results in the decrease of the Al_2O_3/GaN-HEMT and $(Ta_2O_5)_{0.12}(Al_2O_3)_{0.88}$/GaN-HEMT VBOs to 0.3 eV and 0.1 eV, respectively, and the increase of the corresponding CBOs to 2.8 eV and 2.6 eV. Therefore, the post-deposition annealing step used during HEMT processing improves the interface characteristics of the samples by increasing the barrier height to the n-type GaN-HEMT giving potentially lower leakage currents. These results demonstrate that ALD with modulation doping can be used to optimally control the properties of $(Ta_2O_5)_x(Al_2O_3)_{1-x}$ as gate dielectric to achieve both a high-κ and a sufficient CBO to the GaN-HEMT structure for low leakage currents.

[1]R. T. Kemerley, H. B. Wallace, and M. N. Yoder, Proc. IEEE **90**, 1059 (2002).

[2]R. J. Trew, Proc. IEEE **90**, 1032 (2002).

[3]K. Cheng, H. Liang, M. Van Hove, K. Geens, B. De Jaeger, P. Srivastava, X. Kang, P. Favia, H. Bender, S. Decoutere, J. Dekoster, J. I. del Agua Borniquel, S. W. Jun, and H. Chung, Appl. Phys. Express **5**, 011002 (2012).

[4]S. Tripathy, V. K. X. Lin, S. B. Dolmanan, J. P. Y. Tan, R. S. Kajen, L. K. Bera, S. L. Teo, M. K. Kumar, S. Arulkumaran, G. I. Ng, S. Vicknesh, S. Todd, W. Z. Wang, G. Q. Lo, H. Li, D. Lee, and S. Han, Appl. Phys. Lett. **101**, 082110 (2012).

[5]B. De Jaeger, M. Van Hove, D. Wellekens, X. Kang, H. Liang, G. Mannaert, K. Geens, and S. Decoutere, "Au-Free CMOS-Compatible AlGaN/GaN HEMT Processing on 200 mm Si Substrates," in Proceedings of the 24th International Symposium on Power Semiconductor Devices and ICs (IEEE, 2012), pp. 49–52.

[6]D. Christy, T. Egawa, Y. Yano, H. Tokunaga, Y. Yamaoka, A. Ubukata, T. Tabuchi, H. Shimamura, and K. Matsumoto, Appl. Phys. Express **6**, 026501 (2013).

[7]S. Lenci, B. De Jaeger, L. Carbonell, J. Hu, G. Mannaert, D. Wellekens, S. You, B. Bakeroot, and S. Decoutere, IEEE Electron Device Lett. **34**, 1035 (2013).

[8]M. A. Huque, S. A. Eliza, T. Rahman, H. F. Huq, and S. K. Islam, Solid State Electron. **53**, 341 (2009).

[9] Rashmi, A. Kranti, S. Haldar, M. Gupta, and R. S. Gupta, IEEE Trans. Microwave Theory Tech. **51**, 607 (2003).

[10]A. Chakroun, H. Maher, E. Al Alam, A. Souifi, V. Aimez, R. Ares, and A. Jaouad, IEEE Electron Device Lett. **35**, 318 (2014).

[11]W. Saito, M. Kuraguchi, Y. Takada, K. Tsuda, I. Omura, and T. Ogura, IEEE Trans. Electron Devices **52**, 159 (2005).

[12]P. D. Ye, B. Yang, K. K. Ng, J. Bude, G. D. Wilk, S. Halder, and J. C. M. Hwang, Appl. Phys. Lett. **86**, 063501 (2005).

[13]Y. Yue, Y. Hao, Q. Feng, J. Zhang, X. Ma, and J. Ni, Chin. Phys. Lett. **24**, 2419 (2007).

[14]Y. Yue, Y. Hao, J. Zhang, J. Ni, W. Mao, Q. Feng, and L. Liu, IEEE Electron Device Lett. **29**, 838 (2008).

[15]Y. C. Chang, W. H. Chang, Y. H. Chang, J. Kwo, Y. S. Lin, S. H. Hsu, J. M. Hong, C. C. Tsai, and M. Hong, Microelectron. Eng. **87**, 2042 (2010).

[16]G. Ye, H. Wang, S. Arulkumaran, G. I. Ng, R. Hofstetter, Y. Li, M. J. Anand, K. S. Ang, Y. K. T. Maung, and S. C. Foo, Appl. Phys. Lett. **103**, 142109 (2013).

[17]E. Bersch, S. Rangan, R. A. Bartynski, E. Garfunkel, and E. Vescovo, Phys. Rev. B **78**, 085114 (2008).

[18]H. C. Lin, P. D. Ye, and G. D. Wilk, Appl. Phys. Lett. **87**, 182904 (2005).

[19]Y. C. Chang, M. L. Huang, Y. H. Chang, Y. J. Lee, H. C. Chiu, J. Kwo, and M. Hong, "Atomic-layer-deposited Al₂O₃ and HfO₂ on GaN: A comparative study on interfaces and electrical characteristics," in Proceedings of the 17th Biennial International Insulating Films on Semiconductor Conference (Elsevier B.V, 2011), pp. 1207–1210.

[20]C. Adelmann, A. Delabie, B. Schepers, L. N. J. Rodriguez, A. Franquet, T. Conard, K. Opsomer, I. Vaesen, A. Moussa, G. Pourtois, K. Pierloot, M. Caymax, and S. Van Elshocht, Chem. Vap. Deposition **18**, 225 (2012).

[21]E. Atanassova and D. Spasov, Microelect. Reliab. **42**, 1171 (2002).

[22]A. Paskaleva and E. Atanassova, J. Phys. D **39**, 2950 (2006).

[23]E. Atanassova, N. Novkovski, A. Paskaleva, and M. Pecovska-Gjorgjevich, Solid State Electron. **46**, 1887 (2002).

[24]L. S. Yeoh, M. J. Abdullah, and Z. Hassan, Int. J. Adv. Eng. Technol. **III**, 21 (2012), see http://www.technicaljournalsonline.com/ijeat/VOL%20III/IJAET%20VOL%20IIII%20ISSUE%20IV%20%20OCTBER%20DECEMBER%202012/Article%204%20Vol%20III%20issue%20IV%202012.pdf.

[25]N. V. Nguyen, O. A. Kirillov, W. Jiang, W. Wang, J. S. Suehle, P. D. Ye, Y. Xuan, N. Goel, K.-W. Choi, W. Tsai, and S. Sayan, Appl. Phys. Lett. **93**, 082105 (2008).

[26]D. A. Deen, D. F. Storm, R. Bass, D. J. Meyer, D. S. Katzer, S. C. Binari, J. W. Lacis, and T. Gougousi, Appl. Phys. Lett. **98**, 023506 (2011).

[27]J. Yang, B. S. Eller, C. Zhu, C. England, and R. J. Nemanich, J. Appl. Phys. **112**, 053710 (2012).

[28]G. D. Wilk, R. M. Wallace, and J. M. Anthony, J. Appl. Phys. **89**, 5243 (2001).

[29]S. Kimura, Y. Nishioka, A. Shintani, and K. Mukai, J. Electrochem. Soc. **130**, 2414 (1983).

[30]T. L. Duan, J. S. Pan, and D. S. Ang, Appl. Phys. Lett. **102**, 201604 (2013).

[31]J. Robertson and B. Falabretti, J. Appl. Phys. **100**, 014111 (2006).

[32]S. J. Yun, H. Kim, K. Nam, K. Lee, and J. Skarp, J. Vac. Sci. Technol. A **15**, 2993 (1997).

[33]W. J. Maeng and H. Kim, Electrochem. Solid-State Lett. **9**, G191 (2006).

[34]J. Bergsten, A. Malmros, M. Tordjman, P. Gamarra, C. Lacam, M.-A. di Forte-Poisson, and N. Rorsman, Semicond. Sci. Technol. **30**, 105034 (2015).

[35]A. Malmros, N. Rorsman, and H. Blanck, Semicond. Sci. Technol. **26**, 075006 (2011).

[36]E. Simoen, A. Rothschild, B. Vermang, J. Poortmans, and R. Mertens, Electrochem. Solid-State Lett. **14**, H362 (2011).

[37]M. T. Nichols, W. Li, D. Pei, G. A. Antonelli, Q. Lin, S. Banna, Y. Nishi, and J. L. Shohet, J. Appl. Phys. **115**, 094105 (2014).

[38]H. Y. Yu, M. F. Li, B. J. Cho, C. C. Yeo, M. S. Joo, D. Kwong, J. S. Pan, C. H. Ang, J. Z. Zheng, and S. Ramanathan, Appl. Phys. Lett. **81**, 376 (2002).

[39]R. H. French, J. Am. Ceram. Soc. **73**, 477 (1990).

[40]T. V. Perevalov, O. E. Tereshenko, V. A. Gritsenko, V. A. Pustovarov, A. P. Yelisseyev, C. Park, H. H. Jeong, and C. Lee, J. Appl. Phys. **108**, 013501 (2010).

[41]C. Chaneliere, J. L. Autran, R. Devine, and B. Balland, Mater. Sci. Eng. R. **22**, 269 (1998).

[42]R. W. Grant, E. A. Kraut, J. R. Waldrop, and S. P. Kowalczyk, in *Heterojunction Band Discontinuities: Physics and Device Applications*, edited by F. Capasso and G. Margaritondo (North-Holland, Amsterdam, 1987).

[43]E. A. Kraut, R. W. Grant, J. R. Waldrop, and S. P. Kowalczyk, Phys. Rev. Lett. **44**, 1620 (1980).

[44]K. Prabhakaran, T. G. Andersson, and K. Nozawa, Appl. Phys. Lett. **69**, 3212 (1996).

[45]F. G. Bell and L. Ley, Phys. Rev. B **37**, 8383 (1988).

[46]T. E. Cook, Jr., C. C. Fulton, W. J. Mecouch, R. F. Davis, G. Lucovsky, and R. J. Nemanich, J. Appl. Phys. **94**, 7155 (2003).

[47]J. R. Waldrop and R. W. Grant, Appl. Phys. Lett. **68**, 2879 (1996).

[48]Q. Yan, P. Rinke, M. Scheffler, and C. G. Van de Walle, Appl. Phys. Lett. **95**, 121111 (2009).

[49]See supplemental material at http://dx.doi.org/10.1063/1.4939298 for the XPS Al 2p and VBM spectra of the asdeposited and annealed "bulk" oxide samples.

[50]R. L. Anderson, Solid-State Electron. **5**, 341 (1962).

[51]J. Robertson, J. Vac. Sci. Technol. B **18**, 1785 (2000).

[52]W. Mönch, J. Appl. Phys. **109**, 113724 (2011).

[53]B. S. Eller, J. Yang, and R. J. Nemanich, J. Vac. Sci. Technol. A **31**, 050807 (2013).

[54]J. H. Edgar, *Properties of Group III Nitrides* (Institution of Engineering and Technology, London, 1994).

[55]P. D. Ye, G. D. Wilk, B. Yang, J. Kwo, S. N. G. Chu, S. Nakahara, H.-J. L. Gossmann, J. P. Mannaerts, M. Hong, K. K. Ng, and J. Bude, Appl. Phys. Lett. **83**, 180 (2003).

[56]M. Milojevic, F. Aguirre-Tostado, C. L. Hinkle, H. C. Kim, E. M. Vogel, J. Kim, and R. M. Wallace, Appl. Phys. Lett. **93**, 202902 (2008).

[57]X. Qin, H. Dong, B. Brennan, A. Azacatl, J. Kim, and R. M. Wallace, Appl. Phys. Lett. **103**, 221604 (2013).

[58]B. Brennan, X. Qin, H. Dong, J. Kim, and R. M. Wallace, Appl. Phys. Lett. **101**, 211604 (2012).

[59]M. Tajima and T. Hashizume, Jpn. J. Appl. Phys., Part 1 **50**, 061001 (2011).

[60]G. Ye, H. Wang, S. L. G. Ng, R. Ji, S. Arulkumaran, G. I. Ng, Y. Li, Z. H. Liu, and K. S. Ang, Appl. Phys. Lett. **105**, 152104 (2014).

[61]M. Choi, A. Janotti, and D. W. Van, J. Appl. Phys. **113**, 044501 (2013).

[62]B. Eller, J. Yang, and R. Nemanich, J. Electron. Mater. **43**, 4560 (2014).